BIOCHEMISTRY
including biophysical chemistry & molecular biology

Article

pubs.acs.org/biochemistry

Prion Nucleation Site Unmasked by Transient Interaction with Phospholipid Cofactor

Ashley A. Zurawel,[†] Daniel J. Walsh,[†] Sean M. Fortier,[†] Tamutenda Chidawanyika,[†] Suvrajit Sengupta,[§] Kurt Zilm,*[,§] and Surachai Supattapone*[,†,‡]

[†]Departments of Biochemistry and [‡]Medicine, Geisel School of Medicine at Dartmouth, Hanover, New Hampshire 03755, United States

[§]Department of Chemistry, Yale University, New Haven, Connecticut 06520, United States

Supporting Information

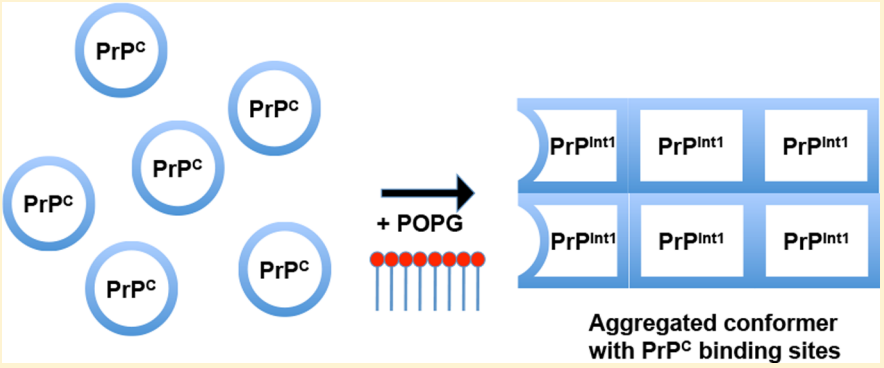

ABSTRACT: Infectious mammalian prions can be formed de novo from purified recombinant prion protein (PrP) substrate through a pathway that requires the sequential addition of 1-palmitoyl-2-oleoyl-sn-glycero-3-phosphoglycerol (POPG) and RNA cofactor molecules. Recent studies show that the initial interaction between PrP and POPG causes widespread and persistent conformational changes to form an insoluble intermediate species, termed PrP^{Int1}. Here, we characterize the mechanism and functional consequences of the interaction between POPG and PrP. Negative-stain electron microscopy of PrP^{Int1} revealed the presence of amorphous aggregates. Pull-down and photoaffinity label experiments indicate that POPG induces the formation of a PrP^{C} polybasic-domain-binding neoepitope within PrP^{Int1}. The ongoing presence of POPG is not required to maintain PrP^{Int1} structure, as indicated by the absence of stoichiometric levels of POPG in solid-state NMR measurements of PrP^{Int1}. Together, these results show that a transient interaction with POPG cofactor unmasks a PrP^{C} binding site, leading to PrP^{Int1} aggregation.

The mechanism of prion diseases such as Creutzfeldt−Jakob disease (CJD), bovine spongiform encephalopathy (BSE), chronic wasting disease (CWD), and scrapie involves the conformational change of the host-encoded prion protein (PrP^{C}) into a misfolded, aggregated, infectious conformer (PrP^{Sc}).[1] Once formed, PrP^{Sc} can seed the conversion of additional PrP^{C} molecules in an exponential-growth process responsible for the pathogenesis and transmission of disease. PrP oligomerization and aggregation appear to be critical steps in prion formation[2] and toxicity.[3,4] In recent years, various experimental approaches have provided valuable insights about the process by which PrP^{C} molecules interact with PrP^{Sc} molecules and undergo induced conformational change into infectious prions.

In one line of investigation, studies using motif-grafted antibodies and tagged PrP peptides identified two linear polybasic domains on PrP^{C} (residues 23−33 and 100−110) as consensus PrP^{Sc}-binding epitopes.[5−7] Moreover, the functional importance of the N-terminal 23−33 polybasic domain was confirmed by showing that a N-truncated (Δ23−28) PrP mutant was unable to bind PrP^{Sc} or to undergo templated conformational change efficiently.[8] Together, these studies argue that the N-terminal polybasic domain of PrP^{C} interacts with the prion nucleation site of PrP^{Sc}.

Much insight into the process of prion formation has also been gained through the development of protocols that enable in vitro PrP^{Sc} formation and propagation. A series of seminal studies showed that PrP^{Sc} molecules[9−11] and infectious prions[12] could be formed in vitro, allowing the conversion process to be studied by using a reductionist approach. Using a reconstitution system, Deleault et al. showed that infectious prions could be formed de novo by subjecting a substrate mixture of purified PrP^{C} (containing stoichiometric amounts of an unidentified copurified lipid but no other proteins or nucleic acids) and synthetic homopolymeric RNA molecules to serial protein-misfolding cyclic amplification (sPMCA).[13] Critically, no PrP^{Sc}

Received: October 31, 2013
Revised: December 11, 2013
Published: December 12, 2013

   dx.doi.org/10.1021/bi4014825 | *Biochemistry* 2014, 53, 68−76

molecules or prion infectivity could be formed using PrP^C alone, showing that cofactor molecules are necessary for efficient prion propagation in vitro. Wang et al. were also able to produce infectious prions de novo using bacterially expressed, refolded, recombinant (rec)PrP substrate combined with the synthetic lipid 1-palmitoyl-2-oleoyl-sn-glycero-3-phosphoglycerol (POPG) and RNA.[14]

To study the mechanism by which cofactor molecules facilitate the formation of infectious PrP^{Sc} molecules de novo, we recently conducted a deuterium-exchange mass spectrometry (DXMS) study to characterize structural changes induced during prion formation in vitro with recPrP and POPG.[15] One important insight provided by this study is that the initial interaction between POPG and recPrP induces major protein conformational changes, some of which appear to persist in the final PrP^{Sc} structure. Here, we investigate the functional consequences and mechanism of this critical interaction using a combination of biophysical and biochemical approaches

EXPERIMENTAL PROCEDURES

Expression and Purification of Recombinant MoPrP and of AviTag PrP. The AviTag PrP sequence was constructed by mutagenesis of a pET-22b(+) expression plasmid encoding the mouse PrP 23−230 sequence originally extracted from pCOMBO3(MoPrP) (Mike Scott, UCSF).[16] The AviTag sequence was added to the C-terminus of the PrP sequence by PCR amplification using primers that included an NdeI restriction enzyme site at the 5′ end of the sequence and a 15 amino acid AviTag sequence added to Ser230 followed by a stop codon and an XhoI site at the 3′ end (5′ AAAAAA-CATATGAAAAAGCGGCCAAAGCCTGGAGGGT 3′ and 5′ AAAACTCGAGTCATTATTCGTGCCATTCGATT-TTCTGAGCCTCGAAGATGTCGTTCAGACCGCC-ACCGGATCTTCTCCCGTCGTAATAG 3′). The PCR product was ligated into the pCR4-TOPO (Invitrogen, San Diego, CA) expression vector, and its sequence was confirmed. The product was digested with NdeI and XhoI and ligated into the pET-22b(+) expression vector for subsequent transformation into *Escherichia coli* Rosetta cells.

Double-isotope-labeled protein for NMR analysis was prepared by growing *E. coli* Rosetta cells transformed with the MoPrP plasmid with DM minimal media containing 1× Mo salt stock (50 mM KH_2PO_4, 30 mM Sodium Citrate, $Na_3C_6H_5O_7{\cdot}2H_2O$, 0.7 mM$CaCl_2{\cdot}2H_2O$, and 10 mM $MgSO_4{\cdot}7H_2O$), 1× DM trace metals stock (100 mM $FeCl_3{\cdot}6H_2O$, 9 mM $ZnCl_2$, 12 mM $CoCl_2{\cdot}6H_2O$, 7.5 mM $CuCl_2{\cdot}2H_2O$,6.8 mM $CaCl_2{\cdot}2H_2O$, 7.45 mM H_3BO_3, and 12 mM HCl), 1× BME vitamins (Sigma, St. Louis, MO), 3 mL of 400× thiamine (Sigma, St. Louis, MO) and 3 g/L of $^{15}NH_4Cl$ and 4 g/L of D-U-C6-glucose (Cambridge Isotope Laboratories Inc., Tewksbury, MA). The protein was subsequently purified using reverse-phase HPLC,[17] and isotope incorporation was verified using MALDI mass spectrometry.

Biotinylation of AviTag PrP. AviTag PrP was biotinylated according to the manufacturer's protocol (Avidity, Aurora, CO). Briefly, Biomix-A and Biomix-B were diluted from their 10× stock concentrations to 1× final concentrations by adding them to AviTag PrP. For 3.2 μg of total protein, 5 μg of BirA enzyme biotin ligase was added to each reaction, and samples were incubated in a thermomixer (Thermo Fisher Scientific, Rockford, IL) at a speed of 750 rpm overnight or for several hours. Five milliliters of 7 kDa zeba spin desalting columns (Thermo Fisher Scientific, Rockford, IL) was used to remove excess biotin. Two-hundred microliters of sample was diluted to a total volume of 500 μL using Assay Buffer (50 mM Tris-HCl, pH 7.5, 200 mM NaCl, 1% Triton, and 1% Tween) before loading onto the column.

Preparation of PrP^{Int1} and PrP^C. PrP^{Int1} was prepared by mixing 180 μL of recombinant PrP protein at a concentration of 0.25 mg/mL resuspended in Milli-Q H_20 with 16 μL of 1-palmitoyl-2-oleoyl-sn-glycero-3- [phospho-rac-(1-glycerol)] (POPG, Avanti Polar Lipids, Alabaster, AL) at a concentration of 2.5 mg/mL, as previously described.[14] POPG was prepared by resuspending lyophilized powder in chloroform, drying under a stream of nitrogen, and resuspending in 20 mM Tris-HCl buffer, pH 7.4, at which point the solution was sonicated at 4 °C in a bath sonicator until it was fully hydrated. The mixture of protein and lipid was incubated for 10 min at room temperature; 7359 μL of MQ H_2O, 500 μL of 5% Triton X-100, and 900 μL of 10× TN Buffer (1.5 M NaCl and 100 mM Tris-HCL, pH 7.5) were added, and the solution was end-over-end rotated for 5 min. Addition of RNA was omitted from the original protocol, and 45 μL of MQ H_2O was added in its place. The sample was centrifuged for 1 h at 100 000*g* in 1 mL aliquots. The supernatant was removed, retaining approximately 70 μL to conserve the integrity of the pellet. The pellet was washed twice with 1 mL of 1% *n*-octyl-*β*-D-glucopyranoside, spinning at 100 000*g* for 1 h after each wash. The resulting pellet was resuspended in 200 μL of assay buffer and sonicated using a Misonix s3000 programmable microplate horn sonicator filled with 350 mL of H_2O heated at 37 °C. The sonicator was set to a power level of 70, and three 15 s bursts were used followed by thorough vortexing for complete resuspension of pellet.

PrP^C was purified from normal mouse brain as previously described.[13]

Polybasic-Domain Peptide Pull-Down Assay. Biotinylated PrP peptide-capture assays were performed using a modified version of a previously described protocol.[5] Streptavidin-coated magnetic beads (Dynabeads M280-Streptavidin, Invitrogen, San Diego, CA) were rinsed four times with assay buffer (50 mM Tris-HCl, pH 7.5, 200 mM NaCl, 1% Triton, and 1% Tween) and diluted 10-fold. The beads were then incubated with 10 μM PBD (KKRPKPGGWNTK-Biotin), PBD* (KKRPKPGGWNTQQSRYPGQGK-Biotin), or CTL (PGQGSPGGNRYK-Biotin) peptide (Invitrogen, Carlsbad, CA) for 1 h at 37 °C while end-over-end rotating and subsequently washed four times with assay buffer before resuspension.

Twenty microliters of PrP^{Int1} was added to 100 μL of resuspended, peptide-conjugated beads, and 80 μL of assay buffer was added so that the total reaction volume was 200 μL. Samples were end-over-end rotated for 1 h at 37 °C. Reactions were then washed four times with 100 μL of assay buffer. Supernatant and wash fractions were retained, and each sample was resuspended in 100 μL of assay buffer. For analysis, equivalent fractions of supernatant, wash, and pellet fractions were loaded on SDS-PAGE gels and transferred to PVDF for immunodetection with PrP-specific antibody 27−33 as previously described.[8]

Photoaffinity Labeling. Photoaffinity peptide (PA-PBD; C-terminally labeled KKRPKPGGWNTK-(KLCBiotin)-(KAzidoBz)-amide, $C_{35}H_{54}N_{11}O_6S$) was incubated with PrP^{Int1} or control PrP samples (at concentrations of 100 μM peptide and 25 ng/μL protein unless otherwise indicated) in 100 μL reaction volumes. Reactions were incubated for 1 h at 37 °C

dx.doi.org/10.1021/bi4014825 | *Biochemistry* 2014, 53, 68−76

using end-over-end rotation. Samples were then aliquoted into a white opaque shallow-well ProxiPlate-96 microplate (PerkinElmer, Waltham, MA), minimizing exposure to ambient light. Samples were photoaffinity labeled in the 96−well plates using a UV Stratalinker 2400 (Stratagene, La Jolla, CA) equipped with 312 nm bulbs in which samples were placed approximately 2.5 cm from the light source. The Stratalinker was utilized in the time mode, and samples were exposed to ultraviolet (UV) light for 0, 1, 3, or 5 min. The resulting photoaffinity-labeled molecules were run on SDS-PAGE, transferred to PVDF, blocked with a 2.5% solution of bovine serum albumin (Fisher Scientific, Pittsburgh, PA), and incubated with streptavidin-conjugated HRP (ThermoFisher Scientific, Rockford, IL) at a 1:10 000 dilution before being washed with TBST and developed with SuperSignal West Femto maximum sensitivity substrate (ThermoFisher Scientific, Rockford, IL).

Amylase and Amyloglucosidase Treatment of recPrP^{Sc}. Recombinant PrP^{Sc} for analysis by electron microscopy was generated, RNase- and protease-digested, purified, and concentrated as previously described.[18] An identical volume of the substrate cocktail (containing recPrP, POPG, and total RNA) not subjected to PMCA was processed in parallel (including protease digestion) to serve as a negative control for the analysis. A mixture of 980 μL of deionized H_2O, 10 μL of α-amylase (Sigma A7095), and 10 μL of amyloglucosidase (Sigma A8220) was filtered through a 0.22 μm filter. The filtered enzyme mixture or 1 mL of H_2O (for mock treatment) was transferred to a new tube containing 20 μL of either processed recPrP^{Sc} or control substrate cocktail. Digestion proceeded for 60 min at 37 °C with shaking at 600 rpm. In parallel, digested and mock-treated samples were centrifuged at 100 000g for 1 h, and pellets were sequentially washed once with 1 mL 1% n-octylglucoside, 8.3 mM Tris, pH 7.5, and 150 mM NaCl and twice with 1 mL of H_2O prior to spotting on grids for electron microscopy. Enzymatic activity under these experimental conditions was confirmed by digestion of GlycoBlue (Invitrogen, Carlsbad, CA).

Electron Microscopy. PrP^{Int1} resuspended in molecular grade H_2O was spotted onto a Formvar-coated 300 mesh copper grid and allowed to absorb for 1 min, after which two wash steps were performed with H_2O. Control samples of PrP^{Int1} with either no PrP protein or, alternatively, with no POPG lipid were prepared according to the sample protocol, replacing either the protein or lipid portion with molecular grade H_2O. The recPrP^{Sc} samples were digested with 5 μg/mL (final concentration) of soluble trypsin (Sigma, St. Louis, MO) overnight at room temperature and then inhibited with 2 mM PMSF (Sigma, St. Louis, MO). The digested recPrP^{Sc} was then spun at 100 000g for 1 h and resuspended in molecular grade H_2O. Samples were stained with 2% uranyl acetate applied for 30 s and then allowed to dry overnight before imaging. Transmission electron microscopy was done at 100 kV using a JEM-1010TEM (JEOL Ltd., Tokyo, Japan) microscope with an integrated AMT digital camera (Advanced Microscopy Techniques, Woburn, MA) to capture images.

NMR Spectroscopy. A sample of uniformly ^{13}C- and ^{15}N-enriched PrP^{Int1} prepared as described in the previous section was centrifuged into a 2.5 mm zirconia magic-angle spinning (MAS) rotor. The sample was held in place with micro-O-ring-sealed sample spacers to ensure that the sample maintained a constant state of hydration.[19] Both ^{13}C and ^{15}N cross-polarization MAS (CPMAS) spectra were obtained from room temperature to −100 °C using a probe of our own construction[20] with pulse sequences described elsewhere.[21] ^{31}P spectra were acquired at −10 °C using a double-resonance 2.5 mm Agilent MAS probe. Two-dimensional $^{13}C-^{13}C$ correlation spectra and $^{15}N-^{13}C$ correlation spectra were also acquired at a temperature of −10 °C. An external-field frequency lock[22] was employed to compensate for field drift. All NMR experiments were performed using a Varian VNMRS instrument operating at a ^{1}H frequency of 799.8 MHz. The magic-angle spinning rate was typically 20 kHz, and ^{1}H decoupling was applied at 110 kHz using either TPPM or XiX modulation. ^{13}C chemical shifts were referenced to tetramethylsilane (TMS) using adamantane as an external reference.[23]

RESULTS

Cofactor Induces PrP Aggregation. We recently characterized the incremental changes in recPrP conformation as it interacts with cofactors during the process of de novo prion formation.[15] An intermediate species (PrP^{Int1}) formed by the rapid interaction between recPrP with POPG at room temperature displays widespread and durable changes in protein conformation[15] and can be purified by ultracentrifugation. We examined the ultrastructure of PrP^{Int1} by negative-stain transmission electron microscopy. Interestingly, POPG appears to induce the formation of irregularly shaped PrP^{Int1} aggregates. At higher magnification, these aggregates appear to be composed of variably stained, smooth-contoured subunits of ~20−30 nm in diameter (Figure 1). Aggregates were not

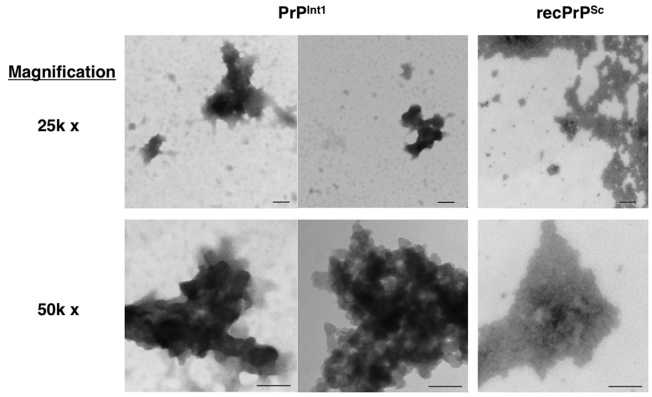

Figure 1. Transmission electron microscopy of PrP^{Int1} and recPrP^{Sc} aggregates. Representative images of PrP^{Int1} and recPrP^{Sc} aggregates are shown at 25 000× and 50 000× magnification. The scale bar at both magnifications is 100 nm.

observed on grids containing samples without POPG or PrP, confirming that interaction between protein and cofactor is necessary to produce aggregates (Figure S1). These results suggest that POPG is able to induce the formation of PrP^{Int1} aggregates. As previously described, the final product of the prion formation protocol (recPrP^{Sc}) also contains aggregates[18] (Figure 1). These aggregates are not glycogen granules, which can be detected in some preparations of total liver RNA,[24] because no protease-resistant aggregates could be seen on grids containing unsonicated substrate cocktail (which includes total RNA) processed in parallel (Figure S2) and also because treatment with amylase did not degrade recPrP^{Sc} aggregates (Figure S2).

Cofactor Unmasks Binding Site for PrP^{C} N-Terminal Polybasic Domain. Binding between PrP^{C} and PrP^{Sc} molecules is an important step in the conversion of cellular

dx.doi.org/10.1021/bi4014825 | Biochemistry 2014, 53, 68−76

PrP^{C} into the PrP^{Sc} conformer. The polybasic domains of PrP^{C} and, in particular, residues 23−33 at the extreme N-terminus have been identified as the primary PrP^{Sc}-binding epitopes.[5−7] Given that POPG is able to induce widespread PrP conformational changes[15] and aggregation (Figure 1), we hypothesized that PrP^{Int1} might contain a binding site for the PrP^{C} polybasic domain. We used a biotinylated peptide representing the N-terminal 23−33 polybasic domain (PBD), which has been previously shown to capture PrP^{Sc} selectively,[5] in streptavidin-based capture assays to measure binding between this domain and PrP^{Int1}. The results show that PBD pulls down ∼70% of total PrP^{Int1}, compared to <10% of input α-helical recPrP (Figure 2A). PrP^{Int1} is also successfully

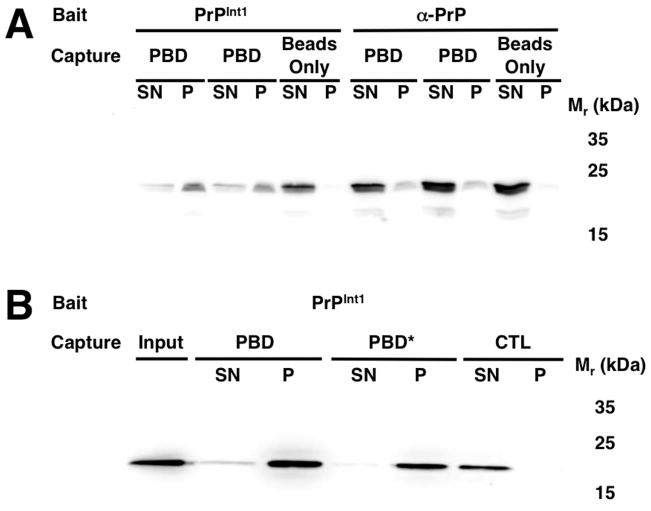

Figure 2. Binding of PrP^{Int1} to polybasic-domain peptide. Western blots probed with anti-PrP antibody 27−33 showing the results of biotinylated peptide capture assays. (A) Input α-helical recPrP or PrP^{Int1} were captured with either PBD peptide-bound streptavidin magnetic beads or beads alone, as indicated. SN, supernatant and P, pellet. (B) Input PrP^{Int1} was captured with biotinylated peptides containing the N-terminal polybasic domain (PBD), an extended and modified version of the N-terminal polybasic domain (PBD*), or a negative control PrP peptide (CTL), as indicated. M_r, relative molecular weight in kilodaltons.

captured by a longer peptide containing the polybasic domain (PBD*) but not by a control peptide (CTL) corresponding to a region of PrP^{C} (residues 39−49) that does not bind PrP^{Sc}[5,7] (Figure 2B). Therefore, the interaction between PrP and POPG appears to unmask a PrP^{C} N-terminal polybasic-domain-binding site, demonstrating how cofactor-induced structural changes can promote intermolecular interactions.

Photoaffinity Labeling of PrP^{Int1} with Polybasic-Domain Peptide. To confirm the results of the pull-down assays, we designed a photoaffinity peptide composed of PrP polybasic domain residues 23−33 conjugated at the C-terminus to biotin and an aryl azide moiety (PA-PBD), and we used UV light to covalently attach this peptide to the PrP^{Int1} conformer (Figure 3A). The photoaffinity-labeled products, representing PA-PBD cross-linked to PrP^{Int1}, can be visualized following SDS-PAGE and transfer to PVDF membranes using streptavidin-conjugated horseradish peroxidase (HRP) to probe for the biotinylated conjugates. The results show that PA-PBD peptide covalently labels PrP^{Int1} more efficiently than either PrP^{C} (Figure 3A) or α-helical recPrP (Figure 3B). Lengthening the duration of UV light exposure increases the

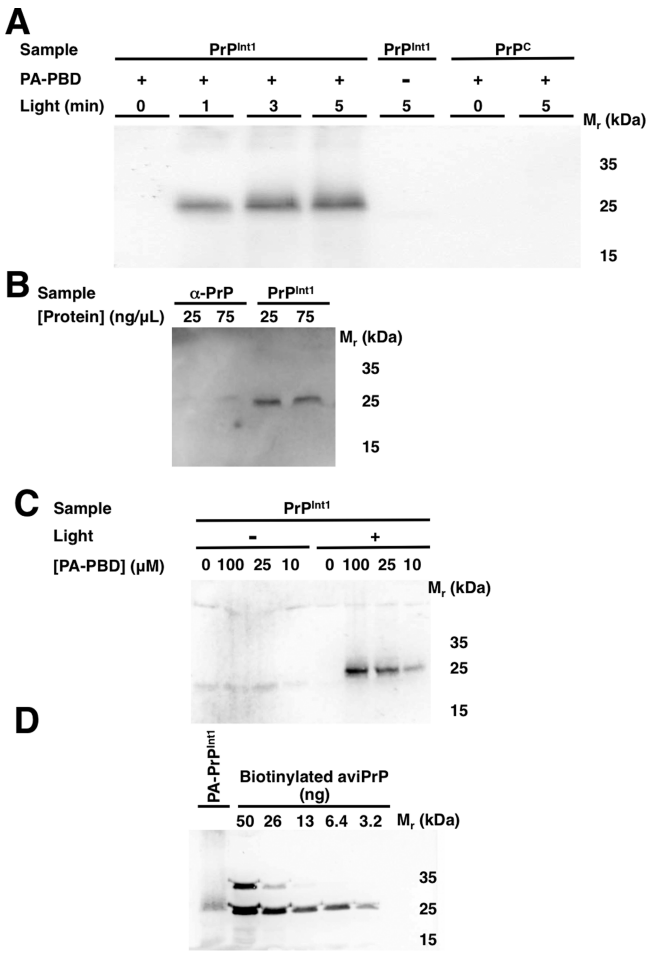

Figure 3. Photoaffinity labeling of various PrP species. Streptavidin-HRP-probed blots of samples photoaffinity labeled with PA-PBD peptide. (A) Samples containing PrP^{Int1} or PrP^{C} were incubated with or without PA-PBD and exposed to UV light for varying time periods, as indicated. (B) Samples containing α-helical PrP or PrP^{Int1} were incubated with PA-PBD and exposed to UV light for 5 min. (C) Samples of PrP^{Int1} were incubated with varying concentrations of PA-PBD, as indicated, and exposed to UV light for 0 or 5 min, as indicated. (D) Sample containing 7 μg of PrP^{Int1} photoaffinity labeled with PA-PBD ($PA\text{-}PrP^{Int1}$) is compared to a standard curve of biotinylated AviTag PrP for reference.

signal intensity of the photoaffinity-labeled band on the blot, whereas no photolabeled bands are seen in the absence of UV light (Figure 3A). Photoaffinity labeling of $PrP^{Int1}$is also enhanced in proportion to increasing concentrations of PA-PBD peptide (Figure 3C). We measured the efficiency of PA-PBD photoaffinity labeling of PrP^{Int1} by using AviTag-PrP, a recombinant PrP fusion protein engineered to contain exactly one biotin adduct per molecule, as a reference standard. By comparing a known amount of photoaffinity-labeled PrP^{Int1} ($PA\text{-}PrP^{Int1}$) to a standard curve representing known concentrations of biotinylated AviTag-PrP, we were able to estimate the stoichiometry of the photoaffinity-labeling reaction of PA-PBD to PrP^{Int1} to be ∼1:2000 (Figure 3D). Potential explanations for the substoichiometric yield of labeled PrP^{Int1} include the presence of inaccessible subunits within PrP^{Int1} aggregates and/or relatively low chemical reactivity of photo-activated pheny azide photoreactive groups.

PrP^{Int1} Does Not Structurally Incorporate Phospholipid. Given the results described above as well as the presence

dx.doi.org/10.1021/bi4014825 | Biochemistry 2014, 53, 68−76

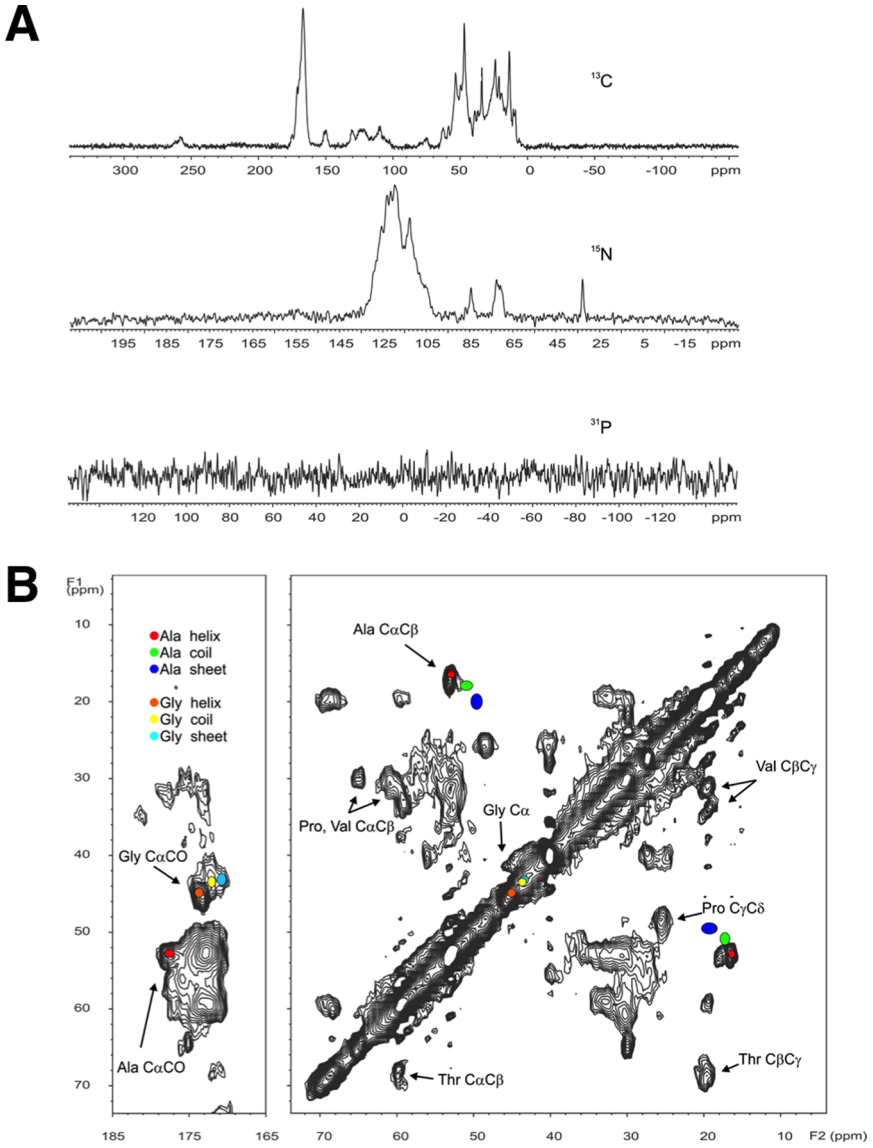

Figure 4. Solid-state NMR spectra. (A) ^{13}C CPMAS spectrum, 64 scans; ^{15}N CPMAS spectrum, 1000 scans; and ^{31}P MAS spectrum, 10 000 scans. All spectra used a 3 s recycle delay and TPPM or XiX decoupling, with a decoupling field strength >100 kHz. (B) Two-dimensional $^{13}C-^{13}C$ correlation spectrum referenced to TMS ($^{13}C-^{13}C$ mixing time of 10 ms, a 2 ms CP time, 512 scans per t_1 point, 256 t_1 points, recycle delay of 3 s, and acquired using TPPI states for quadrature in the indirect dimension). The data set was zero-filled once in each time dimension and apodized using the same Gaussian envelope in each dimension. The 2D contour plot shown has 20 contours spaced in multiples of 1.3 starting just above the noise floor, extending up to the top of all but the most intense auto peaks in the spectrum. A number of characteristic cross peaks are labeled according to the associated amino acid types. As described in the text, characteristic chemical shifts for expected alanine and glycine peaks are denoted for helix, sheet, and coil motifs with color-coded ellipsoids. The glycine Cα diagonal and Cα/CO cross peak for a helical conformation are particularly intense and distinct. Alanine Cα/Cβ cross peaks are seen to also be most consistent with a predominantly helical secondary structure.

of lipid cofactors in protocols capable of producing high-titer infectious PrP^{Sc},[13,14,16] we sought to determine if POPG is incorporated into the PrP^{Int1} macromolecular structure by analyzing the insoluble conformer with solid-state nuclear magnetic resonance (ssNMR) spectroscopy. Using a sample of uniformly ^{13}C- and ^{15}N-enriched PrP^{Int1}, ^{31}P MAS spectra were acquired using both cross-polarization and single-pulse excitation. Regardless of the conditions employed, no ^{31}P signals were in fact observed. Representative ^{13}C, ^{15}N, and ^{31}P spectra obtained at −10 °C for this sample are shown (Figure 4A). Although the ^{13}C and ^{15}N spectra are easily observed in a few scans, no ^{31}P resonances can be found even with an overnight acquisition (Figure 4A). This quantitative conclusion is based on comparison to the ^{31}P signals obtained on a standard sample of ammonium dihydrogen phosphate (ADP). The 6 μL MAS rotor sample volume accommodates 9.4×10^{-5} mol of ADP. Assuming a typical protein density of 1.4 g/cm^3, the same sample cell will hold 3.1×10^{-7} mol of PrPInt1. If there is only one molecule of POPG per PrP^{Int1}, then the ^{31}P NMR signal would have an integrated intensity $\sim 1/300$ of that for the ADP standard sample. The ADP spectrum itself has a relatively narrow line of 0.5 ppm full width at half-maximum and in a single scan has a peak signal 210 times as large as the peak-to-peak noise for the ^{31}P window (Figure 4A). If the POPG were as narrow as the ADP standard, then the 10 000 scan spectrum in the ^{31}P spectrum would have a peak 70 times the noise observed. Even if the line shape were as broad as 5 ppm, the raw peak signal to peak-to-peak noise ratio would still

dx.doi.org/10.1021/bi4014825 | Biochemistry 2014, 53, 68−76

be over 7 and quite easily observed. Because the ^{31}P shift range for phospholipids is fairly narrow and MAS line shapes for POPG are quite generally found to be substantially narrower than 5 ppm, the simplest conclusion consistent with these data is that POPG cannot be present in PrP^{Int1} in stoichiometric amounts.

Cofactor Induces Helical Transition of N-Terminus. The ssNMR analysis of the sample also allowed us to look at the overall structural features of PrP^{Int1}. Analysis of the ^{13}C chemical shifts and spectral intensities demonstrates that PrP^{Int1} is a highly structured macromolecular complex with little molecular mobility and identifiable helical content (Figure 4B). CPMAS ^{13}C spectra detect relatively rigid components in solid samples, whereas Bloch decay MAS spectra will preferentially observe motionally narrowed segments. Regardless of the temperature, the ^{13}C CPMAS and Bloch decay spectra of PrP^{Int1} have essentially identical intensity profiles. This is in stark contrast to results obtained for huPrP23−144 amyloid (no CPMAS signals observed for 23−111)[25] or on Syrian hamster PrP23−231 amyloid (weak or no CPMAS signals observed for 23−129).[26] PrP^{Int1}, therefore, appears to be well-structured, with no evidence for extended highly dynamic segments.

Although the spectra are not well-resolved enough to make much headway on site-specific assignments, several unique patterns for different amino acids are nevertheless readily recognized.[27] Thr, Pro, Ala, and Val Cα to Cβ cross peaks are easily picked out as indicated with arrows (Figure 4B). Gly Cα carbon resonances characteristically appear in the 42−46 ppm window with respect to TMS. The uniquely positioned Gly Cα to CO cross peaks are also quite evident, making this assignment possible, and have an intensity consistent with 37 Gly residues. Because 37 of the 38 Gly residues are in the 23−127 segment, observation of these peaks alone points to the absence of dynamic disorder in the N-terminus.

The chemical shifts observed also provide insight into the elements of secondary structure present. Cα to Cβ cross peaks in many instances can be used to assign secondary structure to particular amino acids.[28] Of the peaks observed, those for Ala, Val, and Gly provide the best discrimination between α-helical, β-sheet, and random-coil motifs. The average Cα, Cβ, and CO ^{13}C chemical shifts for these three amino acid types are indicated as color-coded ellipses in Figure 4B, where the axes of the ellipses drawn indicate the standard deviations reported.[28] The majority of the Gly residues observed here in PrP^{Int1} contribute to the Cα/CO cross peak at 45.4/173.2 ppm from TMS. These coordinates are both approximately 2 ppm higher than those for either β-sheet (43.3/170.6 ppm) or random coil (43.5/171.9 ppm) structures,[28] clearly demonstrating that the observed Gly residues must be present in α-helices. Because 37 of the 38 Gly residues are contained in the N-terminus, it follows that the N-terminus overall has adopted an α-helical conformation in PrP^{Int1}. The Ala residues, six of eight of which are in the N-terminal segment, also have chemical shifts that are most consistent with an α-helical structure of this region.

DISCUSSION

Evidence from reconstitution studies indicates that cofactor molecules play a critical role in facilitating the formation of infectious mammalian prions in vitro.[13,29] High-titer infectious prions can be formed de novo from substrate cocktails containing only purified PrP^{C} and cofactor molecules in the absence of infectious seed,[13] whereas various preparations of PrP^{Sc} and misfolded PrP lacking cofactors display at least 10^5-fold lower levels of specific infectivity.[30−33] One protocol that can be used to produce infectious prions de novo involves exposing recPrP sequentially to POPG and RNA.[14] We recently showed that the interaction between recPrP and POPG causes dramatic changes in recPrP conformation (measured by solvent accessibility by DXMS), some of which are durable (i.e., persist in the final infectious PrP^{Sc} conformer).[15] Previous studies showed that POPG induces β-sheet structure[34−36] and protease resistance.[36] These changes are likely mediated through an interaction between the phospholipid and the central hydrophobic region of PrP encompassing the polymorphic residue 129.[37] Here, we further characterize the mechanism and consequences of recPrP/POPG interaction to help elucidate the role of cofactor molecules in prion formation.

Ultrastructural analysis by electron microscopy revealed that PrP^{Int1}, the intermediate conformation formed by the interaction of recPrP and POPG, appears to be aggregated. The induction of protein aggregation is likely to be a key event in prion formation because infectious prions are invariably insoluble and aggregated. Because POPG is a relatively small molecule (unlike RNA), it likely does not cause aggregation simply by acting as a scaffold between PrP monomers. PrP^{Int1} aggregates differed morphologically from the ∼40−50 nm wormlike structures formed when PrP is mixed with POPG for extended periods of time at 37 °C.[36] It is not known whether such wormlike structures remain eligible for prion formation (i.e., whether addition of RNA and PMCA would produce infectious prions) or whether they represent an off-pathway product.

We performed a series of PrP polybasic-domain peptide-binding experiments to investigate the mechanism by which POPG induces PrP aggregation. Previous studies using a series of overlapping biotinylated peptides or motif-grafted antibodies to walk the linear polypeptide sequence of PrP identified the two PrP polybasic binding domains (residues 23−33 and 100−110)[5−7] as consensus epitopes on PrP^{C} that bind PrP^{Sc}, and removal of residues 23−88 completely inhibits the ability of PrP^{C} to bind PrP^{Sc}.[8] Thus, conjugated PrP23−33 peptides can be used as specific probes to determine whether a PrP conformer is able to bind PrP^{C}. Using this approach, we found that POPG unmasks a PrP^{C} polybasic-domain-binding site in PrP^{Int1} in both capture and photoaffinity experiments. Presumably, the POPG-induced conformational unmasking of this neoepitope facilitates binding of recPrP to PrP^{Int1} and promotes subsequent aggregation. Interestingly, the association between protein aggregates and the N-terminus of PrP^{C} may be a general phenomenon. Resenberger et al.[38] showed that the N-terminus of PrP^{C} also binds and mediates the toxicity of Aβ oligomers[39] and yeast prions[40] in mammalian cells.

To investigate in greater detail the mechanism by which POPG induces structural and functional changes in PrP, we analyzed PrP^{Int1} chemical composition with ssNMR. The lack of phosphorus atoms in recPrP allowed us to determine whether POPG (which contains phosphorus in its headgroup) remains bound to PrP after formation of the PrP^{Int1} conformation or whether the physical interaction between the protein and phospholipid molecules is transient. The results show that POPG is not present in stoichiometric amounts in PrP^{Int1} and therefore we can conclude that POPG induces the conformational changes in PrP through a transient interaction. Once formed, neither PrP^{Int1} structure nor its ability to bind the PrP^{C} polybasic domain depends upon continued POPG

dx.doi.org/10.1021/bi4014825 | Biochemistry 2014, 53, 68−76

occupancy. These results are consistent with those of a previous study in which in situ degradation of an incorporated photolabile nucleic acid cofactor did not alter the strain properties or titer of purified hamster prions produced in vitro[41] and raise the possibility that cofactor molecules may be able to induce the specific structural changes required for infectivity and strain properties in PrP^{Sc} without physically forming a complex with PrP. However, to confirm this important mechanistic point, it will be necessary to perform similar chemical composition determinations of infectious PrP^{Sc} molecules formed with only a single cofactor, such as phosphatidylethanolamine.[16,29] The conformational change of PrP induced by transient interaction with lipid molecules is remarkable but not unprecedented; for example, conformational changes were also observed for the Bax protein exposed to membrane lipids.[42] In the case of PrP aggregation caused by transient interaction with POPG, the structure of the induced aggregation-prone conformer may be stabilized by intermolecular interactions.

Additional analyses of the ssNMR spectra also provided information about certain aspects of PrP^{Int1} conformation. In particular, we were able to deduce that POPG induces the N-terminus, which is unstructured in PrP^{C}, to form a helical structure. These results are consistent with recent DXMS data showing that POPG causes a moderate level of protection from solvent accessibility in the N-terminus of PrP[15] as well as other experiments examining the effects of another anionic phospholipid, lysophosphatidylserine, on recPrP secondary structure.[43] Previous NMR studies show that both α-helical PrP and PrP amyloid fibers possess disordered N-termini[25,26,44,45] and therefore the presence of helical elements in the N-terminus of PrP^{Int1} is unusual. The significance of this finding is unclear, especially because the subsequent addition of RNA during the prion formation process appears to re-expose the N-terminus fully.[15] Previous studies described the ability of the N-terminal PrP region to acquire poly(L-proline) type II helix conformation under several solvent conditions including phospholipids.[46,47] Another study revealed that the N-terminal polybasic region 23−230 controls the physical properties of alpha-recPrP and its aggregation pathways.[48]

Two recent studies showed that noninfectious PrP^{Sc} conformers with a smaller protease-resistant core than infectious PrP^{Sc} could also be formed in a stochastic fashion when recPrP is subjected to sPMCA in the presence of POPG and RNA.[24,49] These conformers are reminiscent of the noninfectious protein-only PrP^{Sc} conformer, which is formed in a stochastic manner upon cofactor withdrawal and also possesses a smaller protease-resistant core than infectious PrP^{Sc}. It would be interesting to perform similar cofactor-withdrawal experiments to determine whether the noninfectious PrP^{Sc} conformers produced in the presence of POPG and RNA are also protein-only conformers formed as a result of suboptimal interactions between the cofactors and recPrP during sPMCA or are truly cofactor-dependent.

The observation that lipid and polyanionic cofactors are required for the formation of highly infectious prions in vitro is consistent with the important role played by lipid rafts for prion formation in living cells[50] as well as the observation that membrane environment influences PrP conformation and stability.[43,51] Raft domains may harbor high concentrations of specific phsopholipid and other cofactor molecules that enable prion formation. Although POPG can be used to facilitate prion formation in vitro,[14] phosphatidylglycerol itself is not likely to be an endogenous prion conversion cofactor in neurons because it is not generally found in the extracellular raft domains where PrP^{C} normally resides.

In conclusion, using a combination of biophysical and biochemical techniques, we have determined that the prion propagation cofactor POPG unmasks a PrP^{C} polybasic-domain-binding site in PrP, inducing PrP aggregation. However, these effects do not appear to require the continued presence of the POPG cofactor in the PrP folding intermediate.

■ ASSOCIATED CONTENT

Supporting Information

Transmission electron microscopy images of control PrP^{Int1} and PrP^{Sc} samples. This material is available free of charge via the Internet at http://pubs.acs.org.

■ AUTHOR INFORMATION

Corresponding Authors

*(K.M.) E-mail: kurt.zilm@yale.edu.

*(S.S.) E-mail: supattapone@dartmouth.edu. Phone: (603) 650-1192. Fax: (603) 650-1193.

Funding

This work was funded by a research grant from the National Institutes of Health (2R01 NS046478) to S.S. and the National Science Foundation (CHE-1012573) to K.Z.

Notes

The authors declare no competing financial interest.

■ ACKNOWLEDGMENTS

We thank Drs. Fei Wang and Jiyan Ma of Ohio State University for providing samples of $recPrP^{Sc}$ and Katie Weng for help constructing the AviTagPrP plasmid. We also thank Charles Daghlian and Louisa Howard of the Dartmouth Electron Microscopy Facility and Suzette Priola and Andrew Timmes for helpful advice.

■ REFERENCES

(1) Prusiner, S. B. (1998) Prions. *Proc. Natl. Acad. Sci. U.S.A. 95*, 13363−13383.

(2) Kim, C., Haldiman, T., Surewicz, K., Cohen, Y., Chen, W., Blevins, J., Sy, M. S., Cohen, M., Kong, Q., Telling, G. C., Surewicz, W. K., and Safar, J. G. (2012) Small protease sensitive oligomers of PrPSc in distinct human prions determine conversion rate of PrP(C). *PLoS Pathog. 8*, e1002835-1−e1002835-12.

(3) Beranger, F., Crozet, C., Goldsborough, A., and Lehmann, S. (2008) Trehalose impairs aggregation of PrPSc molecules and protects prion-infected cells against oxidative damage. *Biochem. Biophys. Res. Commun. 374*, 44−48.

(4) Wagner, J., Ryazanov, S., Leonov, A., Levin, J., Shi, S., Schmidt, F., Prix, C., Pan-Montojo, F., Bertsch, U., Mitteregger-Kretzschmar, G., Geissen, M., Eiden, M., Leidel, F., Hirschberger, T., Deeg, A. A., Krauth, J. J., Zinth, W., Tavan, P., Pilger, J., Zweckstetter, M., Frank, T., Bahr, M., Weishaupt, J. H., Uhr, M., Urlaub, H., Teichmann, U., Samwer, M., Botzel, K., Groschup, M., Kretzschmar, H., Griesinger, C., and Giese, A. (2013) Anle138b: A novel oligomer modulator for disease-modifying therapy of neurodegenerative diseases such as prion and Parkinson's disease. *Acta Neuropathol. 125*, 795−813.

(5) Lau, A. L., Yam, A. Y., Michelitsch, M. M., Wang, X., Gao, C., Goodson, R. J., Shimizu, R., Timoteo, G., Hall, J., Medina-Selby, A., Coit, D., McCoin, C., Phelps, B., Wu, P., Hu, C., Chien, D., and Peretz, D. (2007) Characterization of prion protein (PrP)-derived peptides that discriminate full-length PrPSc from PrPC. *Proc. Natl. Acad. Sci. U.S.A. 104*, 11551−11556.

(6) Moroncini, G., Kanu, N., Solforosi, L., Abalos, G., Telling, G. C., Head, M., Ironside, J., Brockes, J. P., Burton, D. R., and Williamson, R.

A. (2004) Motif-grafted antibodies containing the replicative interface of cellular PrP are specific for PrPSc. *Proc. Natl. Acad. Sci. U.S.A. 101*, 10404−10409.
(7) Solforosi, L., Bellon, A., Schaller, M., Cruite, J. T., Abalos, G. C., and Williamson, R. A. (2007) Toward molecular dissection of PrPC-PrPSc interactions. *J. Biol. Chem. 282*, 7465−7471.
(8) Miller, M. B., Geoghegan, J. C., and Supattapone, S. (2011) Dissociation of infectivity from seeding ability in prions with alternate docking mechanism. *PLoS Pathog. 7*, e1002128-1−e1002128-12.
(9) Bessen, R. A., Kocisko, D. A., Raymond, G. J., Nandan, S., Lansbury, P. T., and Caughey, B. (1995) Non-genetic propagation of strain-specific properties of scrapie prion protein. *Nature 375*, 698−700.
(10) Kocisko, D. A., Come, J. H., Priola, S. A., Chesebro, B., Raymond, G. J., Lansbury, P. T., and Caughey, B. (1994) Cell-free formation of protease-resistant prion protein. *Nature 370*, 471−474.
(11) Kocisko, D. A., Priola, S. A., Raymond, G. J., Chesebro, B., Lansbury, P. T., Jr., and Caughey, B. (1995) Species specificity in the cell-free conversion of prion protein to protease-resistant forms: a model for the scrapie species barrier. *Proc. Natl. Acad. Sci. U.S.A. 92*, 3923−3927.
(12) Castilla, J., Saa, P., Hetz, C., and Soto, C. (2005) In vitro generation of infectious scrapie prions. *Cell 121*, 195−206.
(13) Deleault, N. R., Harris, B. T., Rees, J. R., and Supattapone, S. (2007) Formation of native prions from minimal componenets in vitro. *Proc. Natl. Acad. Sci. U.S.A. 104*, 9741−9746.
(14) Wang, F., Wang, X., Yuan, C. G., and Ma, J. (2010) Generating a prion with bacterially expressed recombinant prion protein. *Science 327*, 1132−1135.
(15) Miller, M. B., Wang, D. W., Wang, F., Noble, G. P., Ma, J., Woods, V. L., Li, S., and Supattapone, S. (2013) Cofactor molecules induce structural transformation during infectious prion formation. *Structure 21*, 2061−2068.
(16) Deleault, N. R., Piro, J. R., Walsh, D. J., Wang, F., Ma, J., Geoghegan, J. C., and Supattapone, S. (2012) Isolation of phosphatidylethanolamine as a solitary cofactor for prion formation in the absence of nucleic acids. *Proc. Natl. Acad. Sci. U.S.A. 109*, 8546−8551.
(17) Breydo, L., Makarava, N., and Baskakov, I. V. (2008) Methods for conversion of prion protein into amyloid fibrils. *Methods Mol. Biol. 459*, 105−115.
(18) Piro, J. R., Wang, F., Walsh, D. J., Rees, J. R., Ma, J., and Supattapone, S. (2011) Seeding specificity and ultrastructural characteristics of infectious recombinant prions. *Biochemistry 50*, 7111−7116.
(19) Martin, R. W., and Zilm, K. W. (2003) Preparation of protein nanocrystals and their characterization by solid state NMR. *J. Magn. Reson. 165*, 162−174.
(20) Martin, R. W., Paulson, E. K., and Zilm, K. W. (2003) Design of a triple resonance magic angle sample spinning probe for high field solid state nuclear magnetic resonance. *Rev. Sci. Instrum. 74*, 3045−3061.
(21) Morcombe, C. R., Gaponenko, V., Byrd, R. A., and Zilm, K. W. (2004) Diluting abundant spins by isotope edited radio frequency field assisted diffusion. *J. Am. Chem. Soc. 126*, 7196−7197.
(22) Paulson, E. K., and Zilm, K. W. (2005) External field-frequency lock probe for high resolution solid state NMR. *Rev. Sci. Instrum. 76*, 026104-1−026104-3.
(23) Morcombe, C. R., and Zilm, K. W. (2003) Chemical shift referencing in MAS solid state NMR. *J. Magn. Reson. 162*, 479−486.
(24) Timmes, A. G., Moore, R. A., Fischer, E. R., and Priola, S. A. (2013) Recombinant prion protein refolded with lipid and RNA has the biochemical hallmarks of a prion but lacks in vivo infectivity. *PLoS One 8*, e71081-1−e71081-15.
(25) Helmus, J. J., Surewicz, K., Nadaud, P. S., Surewicz, W. K., and Jaroniec, C. P. (2008) Molecular conformation and dynamics of the Y145Stop variant of human prion protein in amyloid fibrils. *Proc. Natl. Acad. Sci. U.S.A. 105*, 6284−6289.
(26) Tycko, R., Savtchenko, R., Ostapchenko, V. G., Makarava, N., and Baskakov, I. V. (2010) The alpha-helical C-terminal domain of full-length recombinant PrP converts to an in-register parallel beta-sheet structure in PrP fibrils: Evidence from solid state nuclear magnetic resonance. *Biochemistry 49*, 9488−9497.
(27) Fritzsching, K. J., Yang, Y., Schmidt-Rohr, K., and Hong, M. (2013) Practical use of chemical shift databases for protein solid-state NMR: 2D chemical shift maps and amino-acid assignment with secondary-structure information. *J. Biomol. NMR 56*, 155−167.
(28) Zhang, H. Y., Neal, S., and Wishart, D. S. (2003) RefDB: A database of uniformly referenced protein chemical shifts. *J. Biomol. NMR 25*, 173−195.
(29) Deleault, N. R., Walsh, D. J., Piro, J. R., Wang, F., Wang, X., Ma, J., Rees, J. R., and Supattapone, S. (2012) Cofactor molecules maintain infectious conformation and restrict strain properties in purified prions. *Proc. Natl. Acad. Sci. U.S.A. 109*, E1938−E1946.
(30) Legname, G., Baskakov, I. V., Nguyen, H. O., Riesner, D., Cohen, F. E., DeArmond, S. J., and Prusiner, S. B. (2004) Synthetic mammalian prions. *Science 305*, 673−676.
(31) Colby, D. W., Wain, R., Baskakov, I. V., Legname, G., Palmer, C. G., Nguyen, H. O., Lemus, A., Cohen, F. E., DeArmond, S. J., and Prusiner, S. B. (2010) Protease-sensitive synthetic prions. *PLoS Pathog. 6*, e1000736-1−e10007360-9.
(32) Makarava, N., Kovacs, G. G., Bocharova, O., Savtchenko, R., Alexeeva, I., Budka, H., Rohwer, R. G., and Baskakov, I. V. (2010) Recombinant prion protein induces a new transmissible prion disease in wild-type animals. *Acta Neuropathol. 119*, 177−187.
(33) Kim, J. I., Cali, I., Surewicz, K., Kong, Q., Raymond, G. J., Atarashi, R., Race, B., Qing, L., Gambetti, P., Caughey, B., and Surewicz, W. K. (2010) Mammalian prions generated from bacterially expressed prion protein in the absence of any mammalian cofactors. *J. Biol. Chem. 285*, 14083−14087.
(34) Kazlauskaite, J., Sanghera, N., Sylvester, I., Venien-Bryan, C., and Pinheiro, T. J. (2003) Structural changes of the prion protein in lipid membranes leading to aggregation and fibrillization. *Biochemistry 42*, 3295−3304.
(35) Sanghera, N., and Pinheiro, T. J. (2002) Binding of prion protein to lipid membranes and implications for prion conversion. *J. Mol. Biol. 315*, 1241−1256.
(36) Wang, F., Yang, F., Hu, Y., Wang, X., Wang, X., Jin, C., and Ma, J. (2007) Lipid interaction converts prion protein to a PrP(Sc)-like proteinase K-resistant conformation under physiological conditions. *Biochemistry 46*, 7045−7053.
(37) Wang, F., Yin, S., Wang, X., Zha, L., Sy, M. S., and Ma, J. (2010) Role of the highly conserved middle region of prion protein (PrP) in PrP-lipid interaction. *Biochemistry 49*, 8169−8176.
(38) Resenberger, U. K., Harmeier, A., Woerner, A. C., Goodman, J. L., Muller, V., Krishnan, R., Vabulas, R. M., Kretzschmar, H. A., Lindquist, S., Hartl, F. U., Multhaup, G., Winklhofer, K. F., and Tatzelt, J. (2011) The cellular prion protein mediates neurotoxic signalling of beta-sheet-rich conformers independent of prion replication. *EMBO J. 30*, 2057−2070.
(39) Lauren, J., Gimbel, D. A., Nygaard, H. B., Gilbert, J. W., and Strittmatter, S. M. (2009) Cellular prion protein mediates impairment of synaptic plasticity by amyloid-beta oligomers. *Nature 457*, 1128−1132.
(40) Chernoff, Y. O. (2008) Prion: Disease or relief? *Nat. Cell Biol. 10*, 1019−1021.
(41) Piro, J. R., Harris, B. T., and Supattapone, S. (2011) In situ photodegradation of incorporated polyanion does not alter prion infectivity. *PLoS Pathog. 7*, e1002001-1−e1002001-7.
(42) Yethon, J. A., Epand, R. F., Leber, B., Epand, R. M., and Andrews, D. W. (2003) Interaction with a membrane surface triggers a reversible conformational change in Bax normally associated with induction of apoptosis. *J. Biol. Chem. 278*, 48935−48941.
(43) Morillas, M., Swietnicki, W., Gambetti, P., and Surewicz, W. K. (1999) Membrane environment alters the conformational structure of the recombinant human prion protein. *J. Biol. Chem. 274*, 36859−36865.

(44) Donne, D. G., Viles, J. H., Groth, D., Mehlhorn, I., James, T. L., Cohen, F. E., Prusiner, S. B., Wright, P. E., and Dyson, H. J. (1997) Structure of the recombinant full-length hamster prion protein PrP(29- 231): The N terminus is highly flexible. *Proc. Natl. Acad. Sci. U.S.A. 94*, 13452−13457.
(45) Viles, J. H., Klewpatinond, M., and Nadal, R. C. (2008) Copper and the structural biology of the prion protein. *Biochem. Soc. Trans. 36*, 1288−1292.
(46) Blanch, E. W., Gill, A. C., Rhie, A. G., Hope, J., Hecht, L., Nielsen, K., and Barron, L. D. (2004) Raman optical activity demonstrates poly(L-proline) II helix in the N-terminal region of the ovine prion protein: implications for function and misfunction. *J. Mol. Biol. 343*, 467−476.
(47) Smith, C. J., Drake, A. F., Banfield, B. A., Bloomberg, G. B., Palmer, M. S., Clarke, A. R., and Collinge, J. (1997) Conformational properties of the prion octa-repeat and hydrophobic sequences. *FEBS Lett. 405*, 378−384.
(48) Ostapchenko, V. G., Makarava, N., Savtchenko, R., and Baskakov, I. V. (2008) The polybasic N-terminal region of the prion protein controls the physical properties of both the cellular and fibrillar forms of PrP. *J. Mol. Biol. 383*, 1210−1224.
(49) Zhang, Z., Zhang, Y., Wang, F., Wang, X., Xu, Y., Yang, H., Yu, G., Yuan, C., and Ma, J. (2013) De novo generation of infectious prions with bacterially expressed recombinant prion protein. *FASEB J. 27*, 4768−4775.
(50) Lewis, V., and Hooper, N. M. (2011) The role of lipid rafts in prion protein biology. *Front. Biosci. 16*, 151−168.
(51) DeMarco, M. L., and Daggett, V. (2005) Local environmental effects on the structure of the prion protein. *C. R. Biol. 328*, 847−862.